

# Early excess emission in Type Ia supernovae from the interaction between supernova ejecta and their circumstellar wind

Takashi J. Moriya,<sup>1,2\*</sup> Paolo A. Mazzali,<sup>3,4</sup> Chris Ashall,<sup>5</sup> and Elena Pian<sup>6</sup>

<sup>1</sup>National Astronomical Observatory of Japan, National Institutes of Natural Sciences, 2-21-1 Osawa, Mitaka, Tokyo 181-8588, Japan

<sup>2</sup>School of Physics and Astronomy, Faculty of Science, Monash University, Clayton, Victoria 3800, Australia

<sup>3</sup>Astrophysics Research Institute, Liverpool John Moores University, IC2, Liverpool Science Park, 146 Brownlow Hill, Liverpool L3 5RF, UK

<sup>4</sup>Max-Planck Institute for Astrophysics, Karl-Schwarzschild-Straße 1, 85748 Garching, Germany

<sup>5</sup>Department of Physics, Virginia Tech, 850 West Campus Drive, Blacksburg VA, 24061, USA

<sup>6</sup>INAF, Astrophysics and Space Science Observatory, via P. Gobetti 101, 40129 Bologna, Italy

Accepted 2023 May 04. Received 2023 April 15; in original form 2023 February 08

## ABSTRACT

The effects of the interaction between Type Ia supernova ejecta and their circumstellar wind on the photometric properties of Type Ia supernovae are investigated. We assume that a hydrogen-rich, dense, and extended circumstellar matter (CSM) is formed by the steady mass loss of their progenitor systems. The CSM density is assumed to be proportional to  $r^{-2}$ . When the mass-loss rate is above  $10^{-4} M_{\odot} \text{ yr}^{-1}$  with a wind velocity of  $100 \text{ km s}^{-1}$ , CSM interaction results in an early flux excess in optical light-curves within 4 days of explosion. In these cases, the optical colour quickly evolves to the blue. The ultraviolet flux below  $3000 \text{ \AA}$  is found to have a persistent flux excess compared to Type Ia supernovae as long as CSM interaction continues. Type Ia supernovae with progenitor mass-loss rates between  $10^{-4}$  and  $10^{-3} M_{\odot} \text{ yr}^{-1}$  may not have a CSM that is dense enough to affect spectra to make them Type Ia-CSM, but they may still result in Type Ia supernovae with an early optical flux excess. Because they have a persistent ultraviolet flux excess, ultraviolet light curves around the luminosity peak would be significantly different from those with a low-density CSM.

**Key words:** supernovae: general – circumstellar matter

## 1 INTRODUCTION

Type Ia supernovae (SNe Ia) are thermonuclear explosions of white dwarfs (e.g., Nugent et al. 2011; Bloom et al. 2012). The evolutionary path leading to white dwarf explosions is a long-standing issue in astrophysics (e.g., Maeda & Terada 2016; Livio & Mazzali 2018; Wang 2018; Soker 2019, for recent reviews). Two major paths have been proposed. One is a so-called “single-degenerate” channel in which a white dwarf gains its mass through the accretion from a non-degenerate companion star (e.g., Nomoto 1982). The other path is a “double-degenerate” channel in which coalescence of binary white dwarfs leads to a thermonuclear explosion (e.g., Iben & Tutukov 1984; Webbink 1984).

The two channels predict different properties of circumstellar matter (CSM) around SNe Ia. In the case of the single-degenerate channel, mass transfer from a non-degenerate star to a white dwarf can lead to mass loss (e.g., Chomiuk et al. 2012; Moriya et al. 2019, and references therein). Thus, single-degenerate systems can lead to the formation of an extended dense hydrogen-rich or helium CSM (e.g., Dragulin & Hoefflich 2016). However, the double-degenerate channel involves two white dwarfs. Therefore, no significant mass loss forming a dense extended CSM is expected from such a system before the explosion. Observationally, a fraction of SNe Ia show clear signa-

tures of interaction between the SN Ia ejecta and an extended dense hydrogen-rich or helium CSM in their optical light-curves and spectra (e.g., Hamuy et al. 2003; Dilday et al. 2012; Silverman et al. 2013; Kool et al. 2022; Sharma et al. 2023), and they are likely related to the single-degenerate channel. It is also possible that SN Ia signatures are often hidden in the interaction features and a certain fraction of interacting SNe are linked to SNe Ia (e.g., Leloudas et al. 2015; Jerkstrand et al. 2020). The fact that some SNe Ia tend to appear in star-forming regions also suggests importance of large mass loss in their progenitor systems and implies the existence of dense CSM around SNe Ia (e.g., Bartunov et al. 1994; Anderson et al. 2015; Pavlyuk & Tsvetkov 2016; Hakobyan et al. 2016).

Several observational features have been linked to the possible presence of hydrogen-rich dense CSM around SNe Ia. For example, strong calcium absorption observed in early spectra of SNe Ia has been related to the existence of hydrogen-rich CSM (e.g., Gerardy et al. 2004; Mazzali et al. 2005a,b; Tanaka et al. 2008). Some SNe Ia also show hydrogen emission lines at late phases that could be excited by CSM interaction (e.g., Kollmeier et al. 2019; Valley et al. 2019; Prieto et al. 2020; Elias-Rosa et al. 2021). In addition, narrow, blueshifted sodium absorption lines detected in SNe Ia are suggested to indicate the existence of extended CSM around their progenitors (e.g., Patat et al. 2007; Maguire et al. 2013). The density of extended CSM around SN Ia progenitor systems can also be probed by radio and X-ray observations of SNe Ia. However, no radio and

\* E-mail: takashi.moriya@nao.ac.jp (TJM)

X-ray emission from SNe Ia has been observed (e.g., Chomiuk et al. 2012, 2016; Pérez-Torres et al. 2014; Harris et al. 2016, 2018, 2021; Lundqvist et al. 2020; Russell & Immler 2012; Margutti et al. 2012, 2014; Dwarkadas 2023) except for SN 2020ejj (Kool et al. 2022)<sup>1</sup>. The lack of radio and X-ray detection indicates that the CSM density around SNe Ia is generally not as high as those predicted by the single-degenerate channel, but it is important to note that the inferred CSM density depends on uncertain physics determining the emission properties (e.g., Chomiuk et al. 2016). It is also possible that there is a delay between the accretion phase and explosion in the single-degenerate channel (e.g., Di Stefano et al. 2011; Justham 2011).

In addition to the aforementioned CSM signatures, early emission from SNe Ia is suggested to contain information on progenitor systems of SNe Ia. Recent early SN Ia observations are starting to reveal that some SNe Ia have excess optical emission within several days after the explosions (e.g., Goober et al. 2014; Cao et al. 2015; Marion et al. 2016; Jiang et al. 2017, 2018, 2020, 2021; Hosseinzadeh et al. 2017, 2022; Miller et al. 2018, 2020; Shappee et al. 2019; Li et al. 2019; Dimitriadis et al. 2019; Tucker et al. 2021; Burke et al. 2021; Ashall et al. 2022; Sai et al. 2022; Ni et al. 2022; Srivastav et al. 2022; Lim et al. 2023). The fraction of SNe Ia showing early excess emission is estimated to be  $\sim 20 - 30\%$  (e.g., Deckers et al. 2022; Magee et al. 2022). Early excess emission was originally suggested to be caused by the impact of the SN ejecta on a non-degenerate companion star in the progenitor system, and therefore to constitute evidence in favour of the single-degenerate channel (e.g., Kasen 2010; Kutsuna & Shigezama 2015; Maeda et al. 2014; Liu et al. 2015). Other mechanisms have been proposed to cause early excess emission, such as mixing of  $^{56}\text{Ni}$  to outer layers (e.g., Piro & Morozova 2016; Noebauer et al. 2017; Maeda et al. 2018; Polin et al. 2019; Magee & Maguire 2020; Magee et al. 2021), Doppler line shifts (Ashall et al. 2022), and existence of carbon and oxygen-rich envelope around white dwarfs (e.g., Ashall et al. 2021; Maeda et al. 2023). In addition to the excess emission, early colour evolution is found to have diversity in SNe Ia (e.g., Stritzinger et al. 2018; Bulla et al. 2020; Burke et al. 2022).

Another possible way to produce early excess emission is the interaction between the SN ejecta and a locally produced CSM. Interaction between SN ejecta and a confined, dense CSM composed mostly of carbon and oxygen has been suggested to cause early excess emission in SNe Ia (e.g., Dessart et al. 2014a; Levanon et al. 2015; Levanon & Soker 2017, 2019; Piro & Morozova 2016; Kromer et al. 2016). This type of CSM is expected to form during the merger of two white dwarfs in the double-degenerate channel (e.g., Hachinger et al. 2012; Schwab et al. 2012; Shen et al. 2012; Pakmor et al. 2013; Tanikawa et al. 2015). However, in the case of the single-degenerate channel, extended hydrogen-rich CSM formed by the mass loss from progenitor systems is expected to exist as discussed earlier. In this study, we investigate how the early emission properties of SNe Ia are affected by the interaction between SN ejecta and such an extended hydrogen-rich CSM.

The rest of the paper is organized as follows. We first show our numerical modelling setups and the initial conditions of our numerical simulations in Section 2. We summarize our results in Section 3. We discuss our results in Section 4 and conclude this paper in Section 5.

<sup>1</sup> There is a controversial case of SN 2005ke (Immler et al. 2006; Hughes et al. 2007). SN 2012ca was detected in X-rays (Bochenek et al. 2018), but it may not be a SN Ia (Inserra et al. 2016).

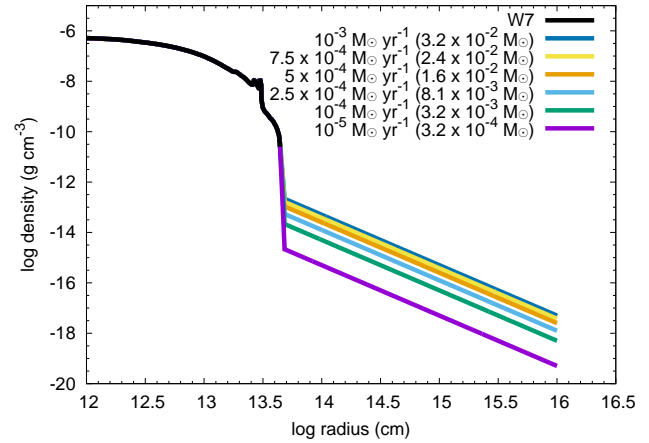


**Figure 1.** Initial density structure in our light-curve calculations. The CSM with  $\rho_{\text{CSM}} \propto r^{-2}$  are attached on top of the W7 density structure at  $4 \times 10^{13}$  cm. The mass-loss rate of each model, as well as the mass in each CSM, is shown in the figure. We assume a wind velocity of  $100 \text{ km s}^{-1}$ .

## 2 METHODS

### 2.1 Numerical modelling

The interaction between SN ejecta and CSM involves the conversion of kinetic energy of SN ejecta to radiation. Thus, it is necessary to treat hydrodynamics and radiation transfer, as well as their mutual effects, simultaneously. We use the one-dimensional multi-frequency radiation hydrodynamics code STELLA (Blinnikov et al. 1998, 2000, 2006) to investigate the consequences of the interaction between SN ejecta and CSM in SNe Ia. STELLA has been used for light-curve modelling of SNe Ia (e.g., Blinnikov et al. 2006; Woosley et al. 2007; Kamiya et al. 2012; Noebauer et al. 2017), including the interaction between SN Ia ejecta and a confined, dense carbon-oxygen CSM (Noebauer et al. 2016). In short, STELLA numerically treats the hydrodynamic equations coupled with radiation, and implicitly solves the time-dependent equations of the angular moments of the radiation intensity averaged over a frequency bin by using the variable Eddington method. STELLA calculates spectral energy distributions (SEDs) at each time step. Multicolour light-curves can be obtained by convolving filter functions with the SEDs. The standard 100 frequency bins in the SED calculations, i.e., from  $1 \text{ \AA}$  to  $5 \times 10^4 \text{ \AA}$  on a log scale, are adopted in this study. STELLA assumes spherical symmetry in calculating hydrodynamic and radiation properties. Although SNe Ia and their CSM may not be spherical (e.g., Liu et al. 2017), our assumption of spherical symmetry would be good enough to obtain the overall properties of CSM interaction features in SNe Ia (cf. Cikota et al. 2019).

### 2.2 Initial conditions

We take the hydrodynamic structure of the W7 model in Nomoto et al. (1984); Thielemann et al. (1986) to represent the SN Ia ejecta. The W7 model is a carbon fast deflagration explosion model of a white dwarf. The W7 model is known to explain the overall properties of SNe Ia (e.g., Nugent et al. 1997; Tanaka et al. 2011), although its nucleosynthesis is known to have some issues (e.g., Iwamoto et al. 1999). Because in the W7 model the SN ejecta properties and the  $^{56}\text{Ni}$  mass, which are the most influential photometric properties of SNe, are overall consistent with SN Ia observations (e.g., Stehle et al.

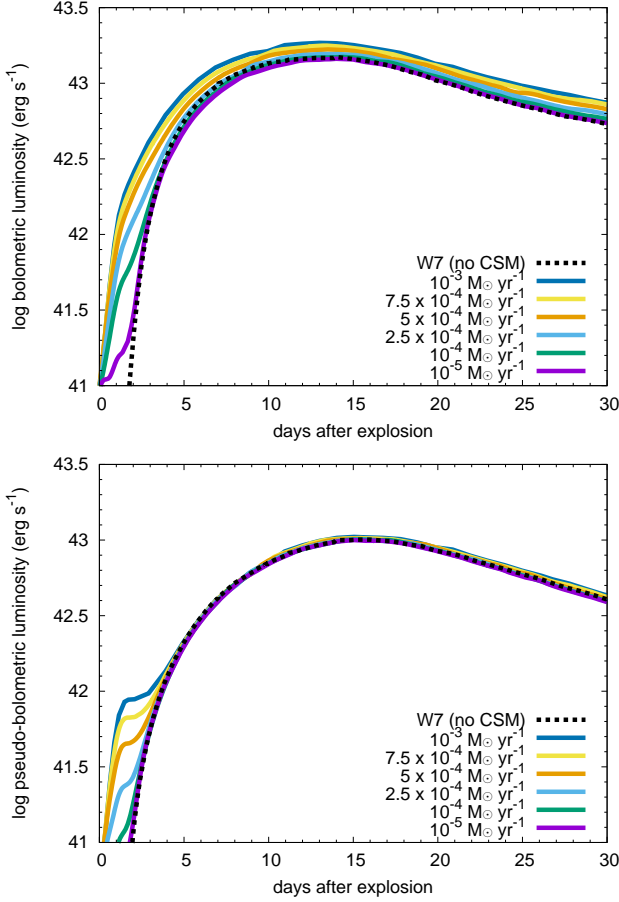


**Figure 2.** Bolometric (top) and pseudo-bolometric (bottom) light-curves obtained from our numerical calculations. The bolometric light-curves include the flux in all the wavelengths and the pseudo-bolometric light-curves are obtained by integrating the optical flux from 3250 Å to 8900 Å.

2005; Mazzali et al. 2008), it is reasonable to adopt it to investigate the effects of CSM interaction in SN Ia photometric properties.

Before colliding on the CSM, the SN Ia ejecta are assumed to expand homologously for  $2 \times 10^4 \text{ sec} \approx 0.2$  days when the outermost layers reach  $4 \times 10^{13} \text{ cm}$ . Because the most extended companion stars in SN Ia progenitor systems are likely red giants having radii of  $\sim 10^{13} \text{ cm}$  (e.g., Hachisu et al. 1996), the CSM interaction may actually start earlier. Still, the collision time is small compared to the timescales of significant changes in photospheric properties. These occur on a timescale of several days, as shown below, such that the assumed collision radius is reasonable.

The CSM structure is attached to the SN ejecta at  $4 \times 10^{13} \text{ cm}$  and extends above. If we assume that the progenitor system experienced steady mass loss, the CSM density can be expressed as

$$\rho_{\text{CSM}} = \frac{\dot{M}}{4\pi v_{\text{wind}} r^2}, \quad (1)$$

where  $\dot{M}$  is the mass-loss rate,  $v_{\text{wind}}$  is the wind velocity, and  $r$  is the radius. The CSM density, which is the most influential parameter in CSM interaction, is determined by  $\dot{M}/v_{\text{CSM}}$ . In this paper, we assume  $v_{\text{wind}} = 100 \text{ km s}^{-1}$  and vary  $\dot{M}$  to investigate the effects of the interaction between SN Ia ejecta and CSM. Our results are not significantly affected by the wind velocity as long as this is smaller than the typical SN Ia ejecta velocity which is much larger than  $1000 \text{ km s}^{-1}$ . Wind velocities of SN Ia progenitors are expected

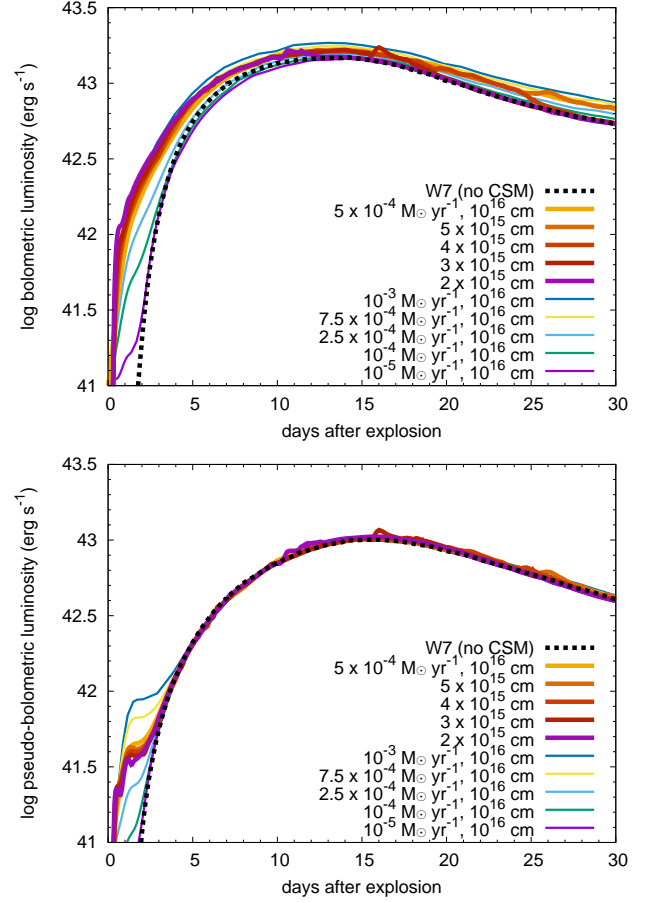


**Figure 3.** Same as Fig. 2, but we additionally show the models with different CSM radii in the case of  $\dot{M} = 5 \times 10^{-4} M_{\odot} \text{ yr}^{-1}$ .

to be  $\sim 10 - 1000 \text{ km s}^{-1}$  (e.g., Chomiuk et al. 2016). The CSM extends to  $10^{16} \text{ cm}$  in our standard models, so that the interaction continues through the peak of the light-curve. The choice of CSM radius does not affect our conclusions as long as the radius is sufficiently large, as discussed below. We also show some models with different CSM radii. The CSM is assumed to have solar composition. The exact composition, however, does not affect our results because the emission properties are mostly determined by the hydrodynamics. Fig. 1 shows the initial density structure of our standard models. Our models cover from  $\dot{M} = 10^{-5} M_{\odot} \text{ yr}^{-1}$  to  $10^{-3} M_{\odot} \text{ yr}^{-1}$ .

The major differences between our initial conditions and those in previous studies of interaction between SN Ia ejecta and CSM concern the density structure. Previous studies considered a CSM formed in the mergers of two white dwarfs and adopt a CSM density structure  $\rho_{\text{CSM}} \propto r^{-3}$  (e.g., Piro & Morozova 2016; Maeda et al. 2018). Thus, the radius of the dense CSM in those studies is smaller than in our model. The CSM composition is also different, but this is not expected to affect interaction-powered light curves, as they are powered mechanically.

## 3 RESULTS

### 3.1 Bolometric light-curves

The top panel of Fig. 2 presents our synthetic bolometric light-curves. We can find that the existence of CSM affects light-curve properties of

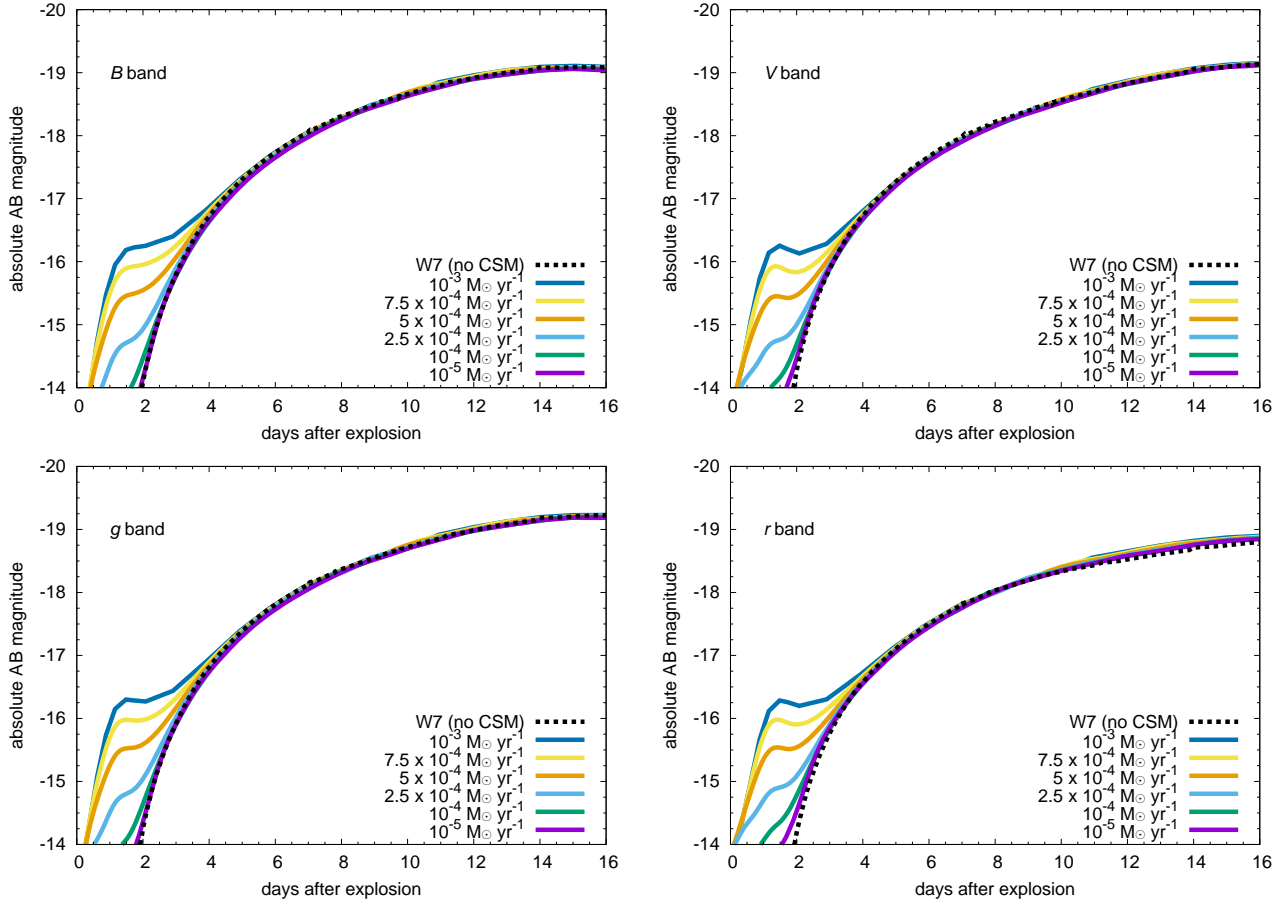


**Figure 4.** Optical light-curves obtained from our numerical calculations.

SNe Ia. When  $\dot{M} \lesssim 2.5 \times 10^{-4} M_{\odot} \text{ yr}^{-1}$ , the bolometric luminosity of SN Ia models with CSM deviate from that without CSM mostly at the earliest phases, within 4 days of explosion. Although CSM interaction continues at later phases, the luminosity from CSM interaction is much less than the luminosity caused by heating from  $^{56}\text{Ni}$  and  $^{56}\text{Co}$  decay. When  $\dot{M} \gtrsim 5 \times 10^{-4} M_{\odot} \text{ yr}^{-1}$ , the luminosity provided by CSM interaction becomes sufficiently high and the bolometric luminosity is higher than that in the model without CSM as long as the interaction continues. Even in these cases, though, the contribution of CSM impact to the luminosity is most significant at the earliest phases, within 4 days of explosion.

The bottom panel of Fig. 2 shows the pseudo-bolometric luminosity evolution that is obtained by integrating the fluxes at optical wavelengths (3250 – 8900 Å). Compared to the bolometric light-curves, excess luminosity due to CSM interaction is only noticeable within 4 days of explosion in all the models. As discussed in the next section, the luminosity excess at later epochs is mostly at ultraviolet (UV) wavelengths. The effect of CSM interaction is only visible at optical wavelengths when  $\dot{M} \gtrsim 10^{-4} M_{\odot} \text{ yr}^{-1}$ , and only in the earliest phases.

Fig. 3 shows the effects of CSM radius on the bolometric and pseudo-bolometric light-curves. The CSM is artificially cut at  $10^{16}$  cm in our models, but the actual outer edge of the CSM is determined by the duration of the mass-loss phase from the progenitor system. Although there are slight differences caused by the CSM radius, the effect of CSM density is found to be much more significant than that of CSM radius. When the CSM radius is too small, however,

CSM interaction does not persist long enough for a luminosity excess to be observed. To summarize, our conclusions in this work are not affected by our assumption on the CSM radius if this is large enough to cause CSM interaction at the earliest phases.

### 3.2 Optical and ultraviolet light-curves

Fig. 4 shows our synthetic light-curves in optical bands. We show the light-curves in the *B* and *V* bands from the Carnegie Supernova Project (CSP, Hamuy et al. 2006) and the *g* and *r* bands from the Zwicky Transient Facility (ZTF, Bellm et al. 2019). As discussed in the previous section, optical light-curves are only affected at the earliest phases within 4 days of explosion. We can find that CSM interaction results in a significant early-phase flux excess in the optical bands when  $\dot{M} \gtrsim 10^{-4} M_{\odot} \text{ yr}^{-1}$ .

The light-curve evolution in UV bands below 3000 Å is presented in Fig. 5. We adopt the *u* band (3000 – 4000 Å) from CSP, and the *uvw2* and *uvw1* bands from *Neil Gehrels Swift Observatory* (Gehrels et al. 2004; Roming et al. 2005), which are sensitive below 3000 Å. The *u* band light-curves have similar properties to those of the optical light-curves with the early-phase excess emission discussed above. However, UV light-curves below 3000 Å show significantly different light-curve features from those found in optical light-curves. In particular, the UV light-curves computed using  $\dot{M} \gtrsim 5 \times 10^{-4} M_{\odot} \text{ yr}^{-1}$  show a persistent flux excess at all phases when interaction is active. The SN UV flux below 3000 Å is usually suppressed in SNe Ia by absorption by Fe-group elements (e.g.,



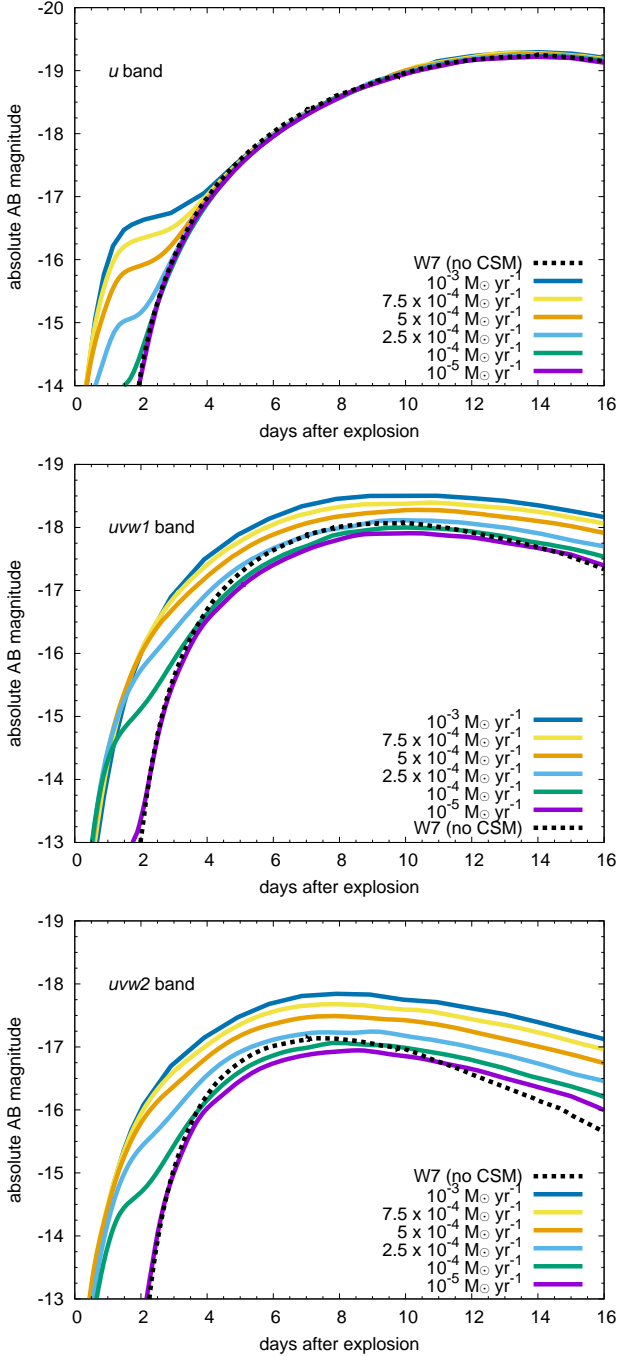


Figure 5. Ultraviolet light-curves obtained from our numerical calculations.

Höflich et al. 1998; Mazzali 2000; Lentz et al. 2000; Kasen et al. 2006; Mazzali et al. 2014; Dessart et al. 2014b). Meanwhile, a large fraction of the radiation from CSM interaction is emitted at the UV wavelengths because of the high shock temperature ( $\sim 10^4$  K, e.g., Moriya et al. 2011). This UV flux is emitted at large radii and can therefore escape. Thus, the effect of CSM interaction is seen mainly at UV wavelengths, and the extra flux from CSM interaction can easily dominate the UV flux of interacting SNe Ia.

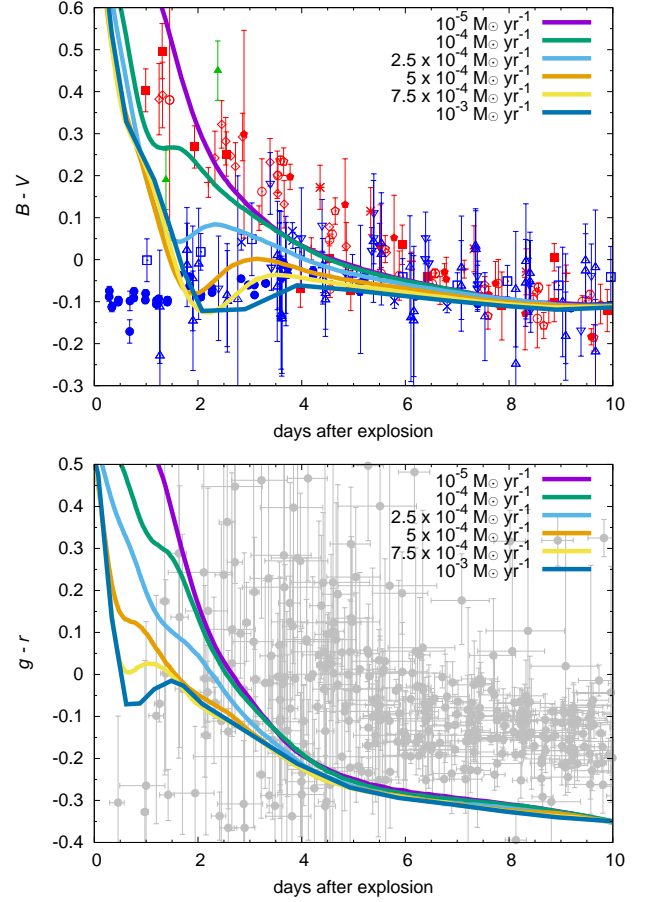


Figure 6. Colour evolution of our synthetic light-curves. The top panel presents the  $B - V$  colour evolution and the bottom panel presents the  $g - r$  colour evolution. We also show the observed colour evolution of SNe Ia from Stritzinger et al. (2018, top) and Bulla et al. (2020, bottom). In the top panel, each SN Ia is plotted with the same symbol as in Stritzinger et al. (2018), and the colour of the symbols is based on the early-phase behavior as defined in Stritzinger et al. (2018). The green symbol is the intermediate case. The details of each SN Ia can be found in Stritzinger et al. (2018). SN 2017cbv is shown by blue circles.

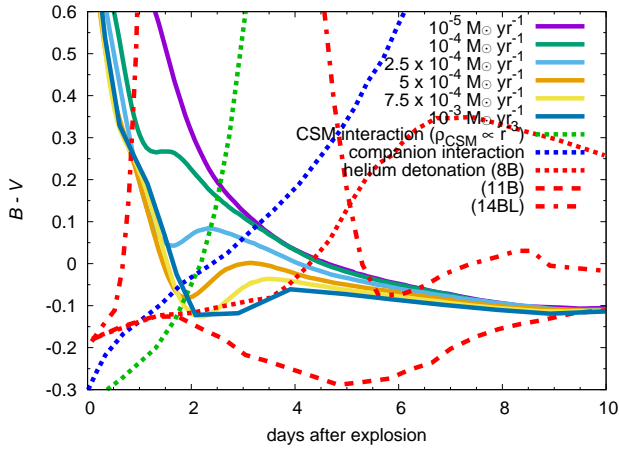
### 3.3 Colour

Fig. 6 shows that the colour evolution of our synthetic SN Ia models is also affected by CSM interaction. When the CSM density is high, SNe Ia are found to become blue more rapidly because of stronger CSM interaction. We discuss a comparison with observations in the next section.

Figure 7 compares the colour evolution of several models predicting early flux excess in SNe Ia from Maeda et al. (2018). A CSM interaction model with a CSM density distribution of  $\rho_{\text{CSM}} \propto r^{-3}$  from a WD merger, a companion interaction model, and three helium detonation models ( $^{56}\text{Ni}$  at outer layers) are compared. Our CSM interaction model ( $\rho_{\text{CSM}} \propto r^{-2}$ ) is found to have a distinct colour evolution compared to other models.

## 4 DISCUSSION

We have shown that the collision between SNe Ia ejecta and an extended CSM caused by a steady wind from the progenitor system leads to a flux excess in the SN optical light-curves in the first 4 days



**Figure 7.** Comparisons of the  $B - V$  colour evolution among different theoretical models predicting early flux excess in SNe Ia. Representative models in Maeda et al. (2018) are presented.

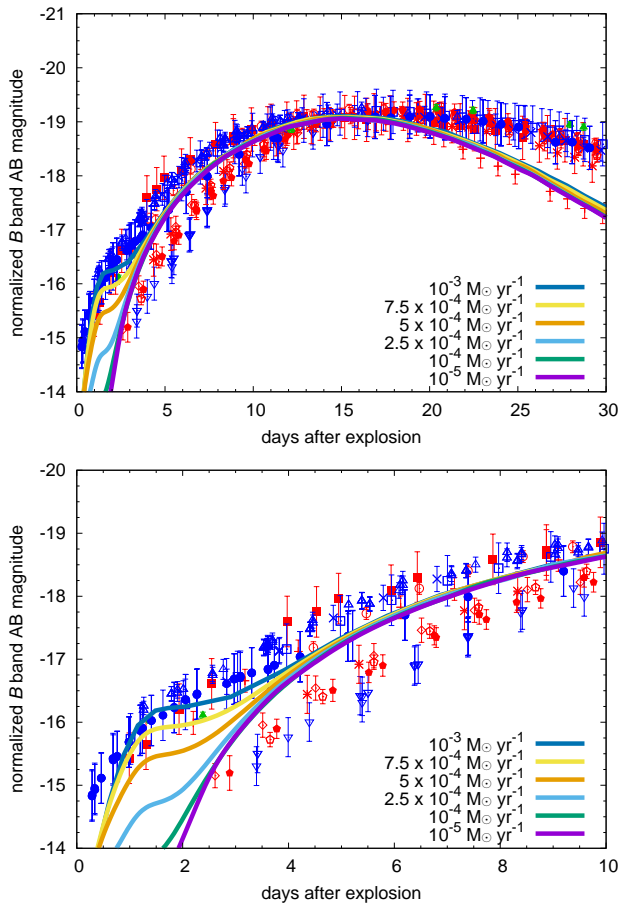


**Figure 8.** Scaled  $B$  band light-curves of the SNe Ia shown in the top panel of Fig. 6, which are taken from Stritzinger et al. (2018). The observed magnitudes are scaled to match the synthetic models at light-curve peak. The top panel shows the light-curves until 30 days after explosion and the bottom panel shows the light-curves until 10 days after explosion. SN 2017cbv is shown as blue circles.

after explosion if  $\dot{M} \gtrsim 10^{-4} M_{\odot} \text{ yr}^{-1}$  with a wind velocity of  $100 \text{ km s}^{-1}$  (Fig. 4). The colour evolution is also affected by CSM interaction (Fig. 6). It has been suggested that there may be distinct populations in colour evolution in the early phases ( $\gtrsim 4$  days) of SNe Ia (Stritzinger et al. 2018), although some studies find the evidence less conclusive (e.g., Bulla et al. 2020). In order to test whether interaction with a CSM could lead to the observed behaviour, the observed colour evolution of SNe Ia is compared to the colour evolution in our synthetic models in Fig. 6. In the case of the  $B - V$  colour evolution presented by Stritzinger et al. (2018), we find that SNe Ia with an early red colour are consistent with the models with  $\dot{M} \lesssim 10^{-4} M_{\odot} \text{ yr}^{-1}$ , while SNe Ia with an early blue colour evolution are more consistent with models with  $\dot{M} \gtrsim 2.5 \times 10^{-4} M_{\odot} \text{ yr}^{-1}$ . The change from red evolution to blue evolution occurs over a small range of  $\dot{M}$  ( $10^{-4} M_{\odot} \text{ yr}^{-1} \lesssim \dot{M} \lesssim 2.5 \times 10^{-4} M_{\odot} \text{ yr}^{-1}$ ).

The ZTF SNe Ia sample (Bulla et al. 2020) does not show the presence of two groups with different  $g - r$  colour evolution (Fig. 6). Our synthetic models match the  $B - V$  evolution of the SNe Ia sample in Stritzinger et al. (2018) well, from early to late phases, but the  $g - r$  colour evolution is quite different at most phases from that of the ZTF SNe Ia as reported by Bulla et al. (2020). We cannot offer a clear reason for this difference. As our numerical calculations do not resolve spectral line features in the  $g$  and  $r$  bands well, some lines in spectra might be responsible for the difference. It is also possible that the explosion dates of the ZTF SN Ia sample, which are estimated by adopting a power-law function, are not well determined, and there might be a systematic shift in the colour evolution.

If the separation in  $B - V$  colour evolution at early phases is the result of a difference in CSM, SNe Ia that are blue at the early phases should always have an early flux excess from CSM interaction. Fig. 8 shows the  $B$  band light-curves of SNe Ia in the Stritzinger’s sample (top panel of Fig. 6). SNe Ia with an early  $B$ -band flux excess tend to have blue colour. In particular, the flux excess and early colour evolution of SN 2017cbv (Hosseinzadeh et al. 2017; Stritzinger et al. 2018) are well explained by our CSM interaction model. However, one SN Ia (SN 2009ig, Blondin et al. 2012; Foley et al. 2012; Marion et al. 2013) with early flux excess has red colour evolution. This suggests that more than one mechanism may be responsible for the early flux excess, as discussed in Section 1. The colour evolution of SN 2017cbv towards the blue is faster than the model prediction. It may be an effect of asphericity in the CSM, allowing photons from the interaction region to escape faster. The discrepancy between the synthetic and observed light curves after peak seen in Fig. 8 may be caused by differences inside the ejecta and it does not affect the early bumps caused by the interaction with the outermost ejecta.

An early flux excess due to CSM interaction requires mass-loss rates from SN Ia progenitor systems of at least  $\dot{M} \gtrsim 10^{-4} M_{\odot} \text{ yr}^{-1}$ , assuming a wind velocity of  $100 \text{ km s}^{-1}$ . Such high mass-loss rates are usually excluded by radio and X-ray observations (Section 1). However, we do know that some SN Ia-CSM progenitor systems had mass-loss rates exceeding  $10^{-3} M_{\odot} \text{ yr}^{-1}$  (e.g., Sharma et al. 2023). It is possible that SN Ia progenitor systems with  $10^{-4} M_{\odot} \text{ yr}^{-1} \lesssim \dot{M} \lesssim 10^{-3} M_{\odot} \text{ yr}^{-1}$  do not exhibit clear CSM interaction signatures in spectra as do SNe Ia-CSM, but only show a flux excess in the light-curves.

SNe Ia with a moderate mass-loss rate such that they only show the early flux excess in optical bands but no spectroscopic signature may still show significant, persistent flux excess also in the UV, and CSM interaction may thus explain some diversity in the UV properties of SNe Ia (e.g., Brown et al. 2012; Brown & Crumpler 2020; Pan et al. 2018, 2020; Srivastav et al. 2022; Sauer et al. 2008). Because 20 – 30% of SNe Ia show early flux excess (e.g., Deckers et al. 2022;

Magee et al. 2022) and there are several mechanisms to cause early flux excess, up to around 10% of SNe Ia may have such early flux excess due to CSM interaction discussed in this paper. Chomiuk et al. (2016) estimated that less than 10% of SNe Ia have mass-loss rates higher than  $10^{-4} M_{\odot} \text{ yr}^{-1}$  based on radio luminosity limits. This is consistent with our estimates of the fraction of SNe Ia with early flux excess from wind interaction. SN Ia progenitor systems with high mass-loss rates may result from optically thick winds (e.g., Kato & Hachisu 1994) or common-envelope winds (e.g., Cui et al. 2022), for example. The fraction of SNe Ia with early flux excess from the CSM interaction is presumably higher than the fraction of SNe Ia-CSM among SNe Ia (0.02 – 0.2% of SNe Ia, Sharma et al. 2023).

Finally, we note that SNe Ia without early flux excess show a rather slow light-curve rise, often referred to as a “dark phase” (e.g., Mazzali et al. 2001; Piro & Nakar 2013). Fitting bolometric light curves with a  $t^2$  function leads to an explosion date estimate of about one day later than the actual explosion date (Fig. 2). A difference of even just one day may be critical in interpreting the earliest photometric and spectroscopic properties of SNe Ia. Interpretation of early observational data needs a careful assessment of the explosion date.

## 5 CONCLUSIONS

We investigated the effect on the photometric properties of SNe Ia of the interaction between the SN ejecta and a surrounding hydrogen-rich, dense, extended CSM. The CSM is assumed to be formed by steady mass loss from the progenitor system. It is assumed to have an extended structure with  $\rho_{\text{CSM}} \propto r^{-2}$  (Eq. 1) and solar metallicity. An early flux excess in optical light-curves is caused by CSM interaction if  $\dot{M} \gtrsim 10^{-4} M_{\odot} \text{ yr}^{-1}$ . UV (below 3000 Å) light-curves are affected significantly and the flux excess there persists as long as CSM interaction continues.

CSM interaction also affects the early colour evolution in SNe Ia. When the CSM density is high enough to cause an early optical flux excess, the optical colour is also found to evolve rapidly towards the blue. Thus, CSM interaction may be partly responsible for the diversity of the early colour evolution that has been seen in SNe Ia. It is possible that a fraction of SNe Ia do not have high enough CSM density for the spectra to display the features of SNe Ia-CSM ( $\dot{M} \gtrsim 10^{-3} M_{\odot} \text{ yr}^{-1}$ ), but still have a sufficient CSM density to cause early-phase flux excess in optical light-curves. This requires ( $10^{-4} M_{\odot} \text{ yr}^{-1} \lesssim \dot{M} \lesssim 10^{-3} M_{\odot} \text{ yr}^{-1}$ ). CSM interaction should also affect the X-ray and radio properties. Multi-wavelength observations of SNe Ia is therefore important in constraining their CSM properties. Such high mass-loss rates are rather extreme even among single-degenerate progenitor systems. However, even though systems with such high mass-loss rates may be rare, they can provide important clues as to the evolutionary path towards SNe Ia. Because the CSM interaction signatures appear clearly in the UV, early SN Ia observations by future ultraviolet satellites such as ULTRASAT<sup>2</sup> and CASTOR<sup>3</sup> will be critical in uncovering the circumstellar environments and progenitor systems of SNe Ia.

<sup>2</sup> <https://www.weizmann.ac.il/ultrasat/>

<sup>3</sup> <https://www.castormission.org/>

## ACKNOWLEDGEMENTS

We thank Benjamin Shappee and Maximilian Stritzinger for useful discussions. This work was supported by the NAOJ Research Coordination Committee, NINS (NAOJ-RCC-22FS-0502, NAOJ-RCC-22FS-0503). PAM and EP are grateful for support and hospitality at NAOJ in Mitaka under program NAOJ-RCC-22FS-0502 and NAOJ-RCC-22FS-0503. TJM is supported by the Grants-in-Aid for Scientific Research of the Japan Society for the Promotion of Science (JP20H00174, JP21K13966, JP21H04997). AC acknowledges support by NASA grant JWST-GO-02114.032-A. Numerical computations were in part carried out on PC cluster at Center for Computational Astrophysics (CfCA), National Astronomical Observatory of Japan.

## DATA AVAILABILITY

The data underlying this article will be shared on reasonable request to the corresponding author.

## REFERENCES

- Anderson J. P., James P. A., Haberman S. M., Galbany L., Kuncarayakti H., 2015, *Publ. Astron. Soc. Australia*, **32**, e019
- Ashall C., et al., 2021, *ApJ*, **922**, 205
- Ashall C., et al., 2022, *ApJ*, **932**, L2
- Bartunov O. S., Tsvetkov D. Y., Filimonova I. V., 1994, *PASP*, **106**, 1276
- Bellm E. C., et al., 2019, *PASP*, **131**, 018002
- Blinnikov S. I., Eastman R., Bartunov O. S., Popolitov V. A., Woosley S. E., 1998, *ApJ*, **496**, 454
- Blinnikov S., Lundqvist P., Bartunov O., Nomoto K., Iwamoto K., 2000, *ApJ*, **532**, 1132
- Blinnikov S. I., Röpke F. K., Sorokina E. I., Gieseler M., Reinecke M., Travaglio C., Hillebrandt W., Stritzinger M., 2006, *A&A*, **453**, 229
- Blondin S., et al., 2012, *AJ*, **143**, 126
- Bloom J. S., et al., 2012, *ApJ*, **744**, L17
- Bochenek C. D., Dwarkadas V. V., Silverman J. M., Fox O. D., Chevalier R. A., Smith N., Filippenko A. V., 2018, *MNRAS*, **473**, 336
- Brown P. J., Crumpler N. R., 2020, *ApJ*, **890**, 45
- Brown P. J., Dawson K. S., Harris D. W., Olmstead M., Milne P., Roming P. W. A., 2012, *ApJ*, **749**, 18
- Bulla M., et al., 2020, *ApJ*, **902**, 48
- Burke J., et al., 2021, *ApJ*, **919**, 142
- Burke J., et al., 2022, arXiv e-prints, p. arXiv:2207.07681
- Cao Y., et al., 2015, *Nature*, **521**, 328
- Chomiuk L., et al., 2012, *ApJ*, **750**, 164
- Chomiuk L., et al., 2016, *ApJ*, **821**, 119
- Cikota A., et al., 2019, *MNRAS*, **490**, 578
- Cui Y., Meng X., Podsiadlowski P., Song R., 2022, *A&A*, **667**, A154
- Deckers M., et al., 2022, *MNRAS*, **512**, 1317
- Dessart L., Blondin S., Hillier D. J., Khokhlov A., 2014a, *MNRAS*, **441**, 532
- Dessart L., Hillier D. J., Blondin S., Khokhlov A., 2014b, *MNRAS*, **441**, 3249
- Di Stefano R., Voss R., Claeys J. S. W., 2011, *ApJ*, **738**, L1
- Dilday B., et al., 2012, *Science*, **337**, 942
- Dimitriadis G., et al., 2019, *ApJ*, **870**, L1
- Dragulin P., Hoefflich P., 2016, *ApJ*, **818**, 26
- Dwarkadas V. V., 2023, *MNRAS*, **520**, 1362
- Elias-Rosa N., et al., 2021, *A&A*, **652**, A115
- Foley R. J., et al., 2012, *ApJ*, **744**, 38
- Gehrels N., et al., 2004, *ApJ*, **611**, 1005
- Gerardy C. L., et al., 2004, *ApJ*, **607**, 391
- Goobar A., et al., 2014, *ApJ*, **784**, L12
- Hachinger S., Mazzali P. A., Taubenberger S., Fink M., Pakmor R., Hillebrandt W., Seitenzahl I. R., 2012, *MNRAS*, **427**, 2057
- Hachisu I., Kato M., Nomoto K., 1996, *ApJ*, **470**, L97

- Hakobyan A. A., et al., 2016, *MNRAS*, **456**, 2848
- Hamuy M., et al., 2003, *Nature*, **424**, 651
- Hamuy M., et al., 2006, *PASP*, **118**, 2
- Harris C. E., Nugent P. E., Kasen D. N., 2016, *ApJ*, **823**, 100
- Harris C. E., et al., 2018, *ApJ*, **868**, 21
- Harris C. E., Chomiuk L., Nugent P. E., 2021, *ApJ*, **912**, 23
- Höflich P., Wheeler J. C., Thielemann F. K., 1998, *ApJ*, **495**, 617
- Hosseinzadeh G., et al., 2017, *ApJ*, **845**, L11
- Hosseinzadeh G., et al., 2022, *ApJ*, **933**, L45
- Hughes J. P., Chugai N., Chevalier R., Lundqvist P., Schlegel E., 2007, *ApJ*, **670**, 1260
- Iben I. J., Tutukov A. V., 1984, *ApJS*, **54**, 335
- Immler S., et al., 2006, *ApJ*, **648**, L119
- Inserra C., et al., 2016, *MNRAS*, **459**, 2721
- Iwamoto K., Brachwitz F., Nomoto K., Kishimoto N., Umeda H., Hix W. R., Thielemann F.-K., 1999, *ApJS*, **125**, 439
- Jerkstrand A., Maeda K., Kawabata K. S., 2020, *Science*, **367**, 415
- Jiang J.-A., et al., 2017, *Nature*, **550**, 80
- Jiang J.-a., Doi M., Maeda K., Shigeyama T., 2018, *ApJ*, **865**, 149
- Jiang J.-a., et al., 2020, *ApJ*, **892**, 25
- Jiang J.-a., et al., 2021, *ApJ*, **923**, L8
- Justham S., 2011, *ApJ*, **730**, L34
- Kamiya Y., Tanaka M., Nomoto K., Blinnikov S. I., Sorokina E. I., Suzuki T., 2012, *ApJ*, **756**, 191
- Kasen D., 2010, *ApJ*, **708**, 1025
- Kasen D., Thomas R. C., Nugent P., 2006, *ApJ*, **651**, 366
- Kato M., Hachisu I., 1994, *ApJ*, **437**, 802
- Kollmeier J. A., et al., 2019, *MNRAS*, **486**, 3041
- Kool E. C., et al., 2022, arXiv e-prints, p. arXiv:2210.07725
- Kromer M., et al., 2016, *MNRAS*, **459**, 4428
- Kutsuna M., Shigeyama T., 2015, *PASJ*, **67**, 54
- Leloudas G., et al., 2015, *A&A*, **574**, A61
- Lentz E. J., Baron E., Branch D., Hauschildt P. H., Nugent P. E., 2000, *ApJ*, **530**, 966
- Levanon N., Soker N., 2017, *MNRAS*, **470**, 2510
- Levanon N., Soker N., 2019, *ApJ*, **872**, L7
- Levanon N., Soker N., García-Berro E., 2015, *MNRAS*, **447**, 2803
- Li W., et al., 2019, *ApJ*, **870**, 12
- Lim G., et al., 2023, arXiv e-prints, p. arXiv:2303.05051
- Liu Z.-W., Moriya T. J., Stancliffe R. J., 2015, *MNRAS*, **454**, 1192
- Liu Z.-W., Stancliffe R. J., Abate C., Matrozos E., 2017, *ApJ*, **846**, 117
- Livio M., Mazzali P., 2018, *Phys. Rep.*, **736**, 1
- Lundqvist P., et al., 2020, *ApJ*, **890**, 159
- Maeda K., Terada Y., 2016, *International Journal of Modern Physics D*, **25**, 1630024
- Maeda K., Kutsuna M., Shigeyama T., 2014, *ApJ*, **794**, 37
- Maeda K., Jiang J.-a., Shigeyama T., Doi M., 2018, *ApJ*, **861**, 78
- Maeda K., Jiang J.-a., Doi M., Kawabata M., Shigeyama T., 2023, *MNRAS*, **521**, 1897
- Magée M. R., Maguire K., 2020, *A&A*, **642**, A189
- Magée M. R., Maguire K., Kotak R., Sim S. A., 2021, *MNRAS*, **502**, 3533
- Magée M. R., et al., 2022, *MNRAS*, **513**, 3035
- Maguire K., et al., 2013, *MNRAS*, **436**, 222
- Margutti R., et al., 2012, *ApJ*, **751**, 134
- Margutti R., Parrent J., Kamble A., Soderberg A. M., Foley R. J., Milisavljevic D., Drout M. R., Kirshner R., 2014, *ApJ*, **790**, 52
- Marion G. H., et al., 2013, *ApJ*, **777**, 40
- Marion G. H., et al., 2016, *ApJ*, **820**, 92
- Mazzali P. A., 2000, *A&A*, **363**, 705
- Mazzali P. A., Nomoto K., Cappellaro E., Nakamura T., Umeda H., Iwamoto K., 2001, *ApJ*, **547**, 988
- Mazzali P. A., Benetti S., Stehle M., Branch D., Deng J., Maeda K., Nomoto K., Hamuy M., 2005a, *MNRAS*, **357**, 200
- Mazzali P. A., et al., 2005b, *ApJ*, **623**, L37
- Mazzali P. A., Sauer D. N., Pastorello A., Benetti S., Hillebrandt W., 2008, *MNRAS*, **386**, 1897
- Mazzali P. A., et al., 2014, *MNRAS*, **439**, 1959
- Miller A. A., et al., 2018, *ApJ*, **852**, 100
- Miller A. A., et al., 2020, *ApJ*, **898**, 56
- Moriya T., Tominaga N., Blinnikov S. I., Baklanov P. V., Sorokina E. I., 2011, *MNRAS*, **415**, 199
- Moriya T. J., Liu D., Wang B., Liu Z.-W., 2019, *MNRAS*, **488**, 3949
- Ni Y. Q., et al., 2022, arXiv e-prints, p. arXiv:2206.12437
- Noebauer U. M., Taubenberger S., Blinnikov S., Sorokina E., Hillebrandt W., 2016, *MNRAS*, **463**, 2972
- Noebauer U. M., Kromer M., Taubenberger S., Baklanov P., Blinnikov S., Sorokina E., Hillebrandt W., 2017, *MNRAS*, **472**, 2787
- Nomoto K., 1982, *ApJ*, **253**, 798
- Nomoto K., Thielemann F. K., Yokoi K., 1984, *ApJ*, **286**, 644
- Nugent P., Baron E., Branch D., Fisher A., Hauschildt P. H., 1997, *ApJ*, **485**, 812
- Nugent P. E., et al., 2011, *Nature*, **480**, 344
- Pakmor R., Kromer M., Taubenberger S., Springel V., 2013, *ApJ*, **770**, L8
- Pan Y. C., Foley R. J., Filippenko A. V., Kuin N. P. M., 2018, *MNRAS*, **479**, 517
- Pan Y. C., Foley R. J., Jones D. O., Filippenko A. V., Kuin N. P. M., 2020, *MNRAS*, **491**, 5897
- Patat F., et al., 2007, *Science*, **317**, 924
- Pavlyuk N. N., Tsvetkov D. Y., 2016, *Astronomy Letters*, **42**, 495
- Pérez-Torres M. A., et al., 2014, *ApJ*, **792**, 38
- Piro A. L., Morozova V. S., 2016, *ApJ*, **826**, 96
- Piro A. L., Nakar E., 2013, *ApJ*, **769**, 67
- Polin A., Nugent P., Kasen D., 2019, *ApJ*, **873**, 84
- Prieto J. L., et al., 2020, *ApJ*, **889**, 100
- Roming P. W. A., et al., 2005, *Space Sci. Rev.*, **120**, 95
- Russell B. R., Immler S., 2012, *ApJ*, **748**, L29
- Sai H., et al., 2022, *MNRAS*, **514**, 3541
- Sauer D. N., et al., 2008, *MNRAS*, **391**, 1605
- Schwab J., Shen K. J., Quataert E., Dan M., Rosswog S., 2012, *MNRAS*, **427**, 190
- Shappee B. J., et al., 2019, *ApJ*, **870**, 13
- Sharma Y., et al., 2023, arXiv e-prints, p. arXiv:2301.04637
- Shen K. J., Bildsten L., Kasen D., Quataert E., 2012, *ApJ*, **748**, 35
- Silverman J. M., et al., 2013, *ApJS*, **207**, 3
- Soker N., 2019, *New Astron. Rev.*, **87**, 101535
- Srivastav S., et al., 2022, arXiv e-prints, p. arXiv:2211.10544
- Stehle M., Mazzali P. A., Benetti S., Hillebrandt W., 2005, *MNRAS*, **360**, 1231
- Stritzinger M. D., et al., 2018, *ApJ*, **864**, L35
- Tanaka M., et al., 2008, *ApJ*, **677**, 448
- Tanaka M., Mazzali P. A., Stanishev V., Maurer I., Kerzendorf W. E., Nomoto K., 2011, *MNRAS*, **410**, 1725
- Tanikawa A., Nakasato N., Sato Y., Nomoto K., Maeda K., Hachisu I., 2015, *ApJ*, **807**, 40
- Thielemann F. K., Nomoto K., Yokoi K., 1986, *A&A*, **158**, 17
- Tucker M. A., et al., 2021, *ApJ*, **914**, 50
- Vallely P. J., et al., 2019, *MNRAS*, **487**, 2372
- Wang B., 2018, *Research in Astronomy and Astrophysics*, **18**, 049
- Webbink R. F., 1984, *ApJ*, **277**, 355
- Woosley S. E., Kasen D., Blinnikov S., Sorokina E., 2007, *ApJ*, **662**, 487

This paper has been typeset from a  $\text{\TeX}/\text{\LaTeX}$  file prepared by the author.